Transition-State Analysis of AMP Deaminase†

David J. Merkler,‡ Paul C. Kline, Paul Weiss,§ and Vern L. Schramm*

Department of Biochemistry, Albert Einstein College of Medicine of Yeshiva University, 1300 Morris Park Avenue, Bronx, New York 10461

Received June 29, 1993; Revised Manuscript Received September 20, 1993®

ABSTRACT: The transition state of the allosteric AMP deaminase from *Saccharomyces cerevisiae* has been characterized by ^{14}C and ^{15}N V_{max}/K_m heavy-atom kinetic isotope effects. The primary 6-^{14}C isotope effect was measured with [6-^{14}C]AMP, and the 6-^{15}N primary isotope effect was measured by isotope ratio mass spectrometry using the natural abundance of ^{15}N in AMP and by using ^{15}N release from ATP as a slow substrate. Isotope effects for AMP as the substrate were measured in the presence and absence of ATP as an allosteric activator and GTP as an allosteric inhibitor. Kinetic isotope effects with [6-^{14}C]AMP were 1.030 ± 0.003, 1.038 ± 0.004, and 1.042 ± 0.003 in the absence of effectors and in the presence of ATP and GTP, respectively. Isotope effects for [6-^{15}N]AMP averaged 1.010 ± 0.002. Allosteric activation increased the ^{15}N isotope effect to 1.016 ± 0.003. A primary ^{15}N kinetic isotope effect with ATP, which has a V_{max}/K_m 10^{-6} that for AMP, was 1.013 ± 0.001. The presence of D_2O as solvent caused a marginally significant decrease in the [6-^{15}N]AMP kinetic isotope effect from 1.011 ± 0.001 to 1.007 ± 0.002. Previous studies have established that the solvent D_2O effect is inverse (0.34) for slow substrates with two or more protons transferred prior to transition state formation and remains inverse (0.79) with AMP as substrate [Merkler, D. J., & Schramm, V. L. (1993) *Biochemistry 32*, 5792–5799]. Bond vibrational analysis was used to identify transition states for AMP deaminase that are consistent with all kinetic isotope effects. Fully concerted reaction mechanisms can be eliminated, since these would result in normal D_2O solvent isotope effects and are inconsistent with ^{14}C and ^{15}N kinetic isotope effects. The transition state most consistent with the data is characterized by an attacking hydroxyl with a bond order near 0.8, a fully bonded NH_2, nearly complete conversion to sp^3 at C6, and highly asymmetric, nearly complete protonation of N1. This transition state leads to the formation of a short-lived tetrahedral intermediate. Formation of the tetrahedral intermediate is slow, while protonation of NH_2 in the intermediate and departure of NH_3 occur in rapid steps.

Adenosine 5′-monophosphate deaminase from baker's yeast (AMP aminohydrolase, EC 3.5.4.6) catalyzes the following reaction:

$$AMP + H_2O \underset{-GTP}{\overset{+ATP}{\rightarrow}} IMP + NH_3$$

where ATP is an allosteric activator and GTP is an allosteric inhibitor (Murakami, 1979; Yoshino et al., 1979; Yoshino & Murakami, 1980, 1986, 1988; Merkler et al., 1989). The gene for AMP deaminase encodes for a protein of 810 amino acids, more than double the size of the 358 amino acid protein required for the analogous reaction catalyzed by mouse adenosine deaminase (Meyer et al., 1989; Yeung et al., 1985). The C-terminal portion of the yeast AMP deaminase shows significant homology to adenosine deaminase. Recently, the mouse adenosine deaminase has been analyzed by X-ray crystallography (Wilson et al., 1991; Scharff et al., 1992; Wilson & Quiocho, 1993). Comparison of the amino acid sequences reveals a striking identity in the amino acids which contact the tightly bound zinc, the purine base, and the ribose (Merkler & Schramm, 1993). These results provide structural evidence that the catalytic domains of the enzymes may function by similar mechanisms. The substrate-binding properties of the enzymes differ since a lysine is part of the sequence which is proposed to interact with the 5′-phosphate region of AMP in yeast AMP deaminase, while a leucine occupies this position in adenosine deaminase. Adenosine is bound to adenosine deaminase more tightly than AMP binds to AMP deaminase either in the presence or absence of allosteric effectors (Merkler et al., 1989; Kurz et al., 1992). AMP, IMP, and NH_3 are in rapid exchange with AMP deaminase, giving a rapid-equilibrium random kinetic mechanism (Merkler & Schramm, 1993). Substrate bound to the enzyme has a low commitment factor for catalysis, making this system suitable for transition-state analysis by kinetic isotope effects [e.g., Northrop (1981)].

An unresolved feature of the catalytic mechanism of AMP deaminase is the nature of the transition state. The crystallography studies of adenosine deaminase with bound purine riboside revealed that enzyme-bound zinc activates the attacking water nucleophile which reacts to form hydrated purine riboside at the catalytic site (Wilson et al., 1991). This structure establishes that a departing NH_3 is not required for hydroxide attack. The crystal structure of adenosine deaminase with 1-deazaadenosine reveals a zinc-bound hydroxyl poised for attack, but not yet interacting with the purine (Wilson & Quiocho, 1993). Thus, protonation of N1 is required for the addition of the hydroxyl at C6. With adenosine as the substrate for adenosine deaminase, it has been proposed that hydroxide attacks to form an intermediate with the tetrahedral carbon at C6, followed by protonation of NH_2 and departure of NH_3 to form the product (Weiss et al., 1987; Kurz et al., 1992). Formation of the intermediate

† This work was supported by NIH Research Grants GM21083 (V.L.S.) and GM18938 (W. W. Cleland, University of Wisconsin) and postdoctoral fellowship GM10599 (D.J.M.).

* Corresponding author.

‡ Current address: Analytical Protein & Organic Chemistry Group, Unigene Laboratories, Inc. 110 Little Falls Road, Fairfield, NJ 07004.

§ Current address: Department of Biochemistry, University of Wisconsin, Madison, WI 53705.

® Abstract published in *Advance ACS Abstracts*, November 15, 1993.

0006-2960/93/0432-12993$04.00/0

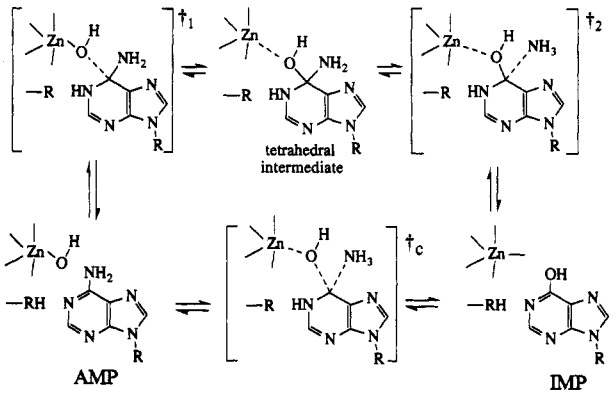

FIGURE 1: Reaction paths for hydrolytic deamination of AMP by AMP deaminase. The upper pathway shows a stepwise conversion with a tetrahedral intermediate characterized by full-bonded hydroxyl and amino groups. The first transition state ($\dagger_1$) results from the attack of the hydroxyl, and the second ($\dagger_2$) results from NH_3 departure. The lower pathway shows a concerted mechanism with simultaneous hydroxide attack and NH_3 departure. The concerted transition state ($\dagger_c$) has partially bonded hydroxyl and NH_3 groups at the transition state. The enzymatic proton donor (RH) is Glu633, and the substituent R is ribose 5-phosphate.

and protonation of the leaving group to form NH_3 have been proposed to occur rapidly for adenosine deaminase (Weiss et al., 1987). This mechanism is in conflict with earlier studies with adenosine deaminase from different sources, which established that V_{max} rates were nearly equivalent when NH_3, Cl, or OCH_3 was the leaving group, despite a range of 10^5 in leaving group potential. These studies support a common slow step of hydroxyl attack (Wolfenden, 1969). Similar studies were not successful with yeast AMP deaminase because of the restricted substrate specificity (Merkler & Schramm, 1993). Proton motion at the transition states of both adenosine and AMP deaminases is limited since solvent kinetic isotope effects for both enzymes are unity or inverse (Weiss et al., 1987; Merkler & Schramm, 1993).

In addition to the mechanisms proposed above, a concerted attack by hydroxide with coincident departure of NH_3 is also a mechanistic possibility for AMP deaminase. These reaction pathways are shown schematically in Figure 1. The reaction type is classified as an aromatic addition–elimination, which implies the formation of an intermediate (March, 1984). The lifetime of the tetrahedral intermediate characterizes the reaction type since as the lifetime approaches zero, the mechanism changes from addition–elimination to concerted nucleophilic displacement. A range of intermediate possibilities obviously exists, with variations in the synchrony of hydroxide attack and NH_3 loss. The purpose of the experiments reported here was to examine the transition-state structure for yeast AMP deaminase.

The mechanism of AMP deamination is determined here by the use of ^{14}C and ^{15}N heavy-atom kinetic isotope effects and bond energy bond order vibrational analysis (Sims & Lewis, 1984). Both the nitrogen leaving group and the carbon that is attacked by zinc-activated water can be analyzed by kinetic isotope effects, provided that bond breaking is among the highest energetic barriers of the reaction coordinate (Northrop, 1981). Steady-state rate analysis which reported that the kinetic mechanism of yeast AMP deaminase is rapid-equilibrium (Merkler et al., 1989) has been confirmed by the effects of pH on the kinetic constants for substrate and a competitive inhibitor (Merkler & Schramm, 1993). These features, plus the ability to use ATP as a very slow substrate, provide the properties required for the analysis of the transition-state structure by kinetic isotope effects.

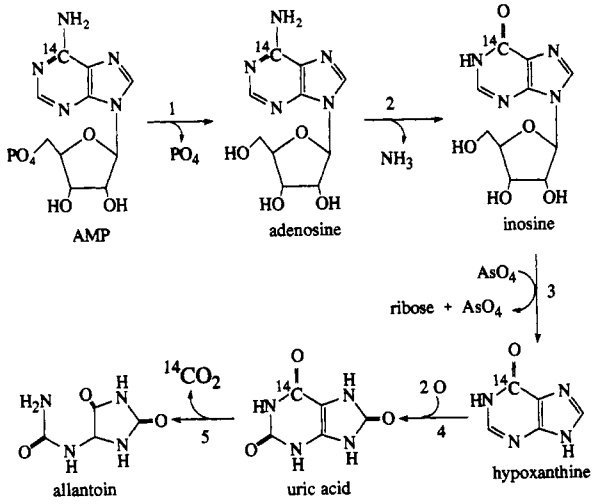

FIGURE 2: Enzymatic degradation of [6-^{14}C]AMP for proof of radiolabel. Radiolabeled AMP was incubated with alkaline phosphatase (1), adenosine deaminase (2), purine nucleoside phosphorylase (3), xanthine oxidase (4), and urate oxidase (5) under the conditions described in Materials and Methods. Each intermediate was analyzed by HPLC for radioactivity.

MATERIALS AND METHODS

Materials. AMP deaminase was purified from commercial baker's yeast by the method of Merkler et al. (1989). Unless otherwise noted, specific activities exceeded 450 μmol/min/mg for all enzyme preparations when assayed at 30 °C. Calf intestinal adenosine deaminase, porcine liver uricase, buttermilk xanthine oxidase, purine nucleoside phosphorylase, and alkaline phosphatase were from Sigma and were used without further purification. D_2O was from Aldrich or Cambridge Isotope Laboratories. [6-^{3}H]Glucose was purchased from New England Nuclear or Amersham.

Nucleotides. All nucleosides and nucleotides were of the highest grade available from Sigma, Aldrich, or Calbiochem. [6-^{14}C]Adenine was purchased from ICN and enzymatically converted to [6-^{14}C]AMP (Parkin et al., 1984). [5′-^{3}H]AMP was enzymatically synthesized from [6-^{3}H]glucose (Parkin et al., 1984).

Initial Rate Studies. Deamination of AMP to IMP and NH_3 was measured using the spectrometric assay previously described (Merkler et al., 1989) or the colorimetric assay for ammonia (Chaney & Marbach, 1962). The buffer for enzyme assays was 30 mM HEPES[1] (pH 7.0) or 50 mM triethanolamine–hydrochloride (TEA–HCl) (pH 7.0). Reaction mixtures also contained 100 mM KCl, 100 μM dithiothreitol, 100 μM ATP, and the desired concentrations of AMP. For solvent isotope effect studies, assay mixtures without nucleotides were lyophilized to dryness and resuspended in the appropriate volume of D_2O. Stocks of nucleotides were prepared in D_2O. No change in the ultraviolet absorbance properties was observed for the conversion of AMP to IMP in H_2O compared to D_2O.

Proof of Structure for [6-^{14}C]AMP. Analysis of the ^{14}C content at the C6 position of AMP followed the enzymatic degradation procedure outlined in Figure 2. Approximately

[1] The solvent inventory studies which gave the large inverse D_2O isotope effect of 0.34 ± 0.02 with dAMP as substrate (Merkler & Schramm, 1993) showed a curved response of V_{max}/K_m to the fraction of D_2O solvent, consistent with two or more proton transfers (Kiick, 1991). A reviewer questioned the nature of the D_2O solvent effects with AMP as substrate. The solvent D_2O isotope effect with AMP is small, at 0.79 ± 0.11; thus, it was not experimentally possible to determine the degree of curvature in plots of V_{max}/K_m as a function of the fraction of D_2O solvent.

3×10^5 cpm of [6-^{14}C]AMP in 1.0 mL of 10 mM CHES (pH 9.0), 2.5 mM AMP (unlabeled, added as a carrier), and 1.5 units of alkaline phosphatase (calf intestine) was incubated at 37 °C for 2 h to quantitatively convert AMP to adenosine. The solution was adjusted to pH 7.2 with HCl, 100 μL of 100 mM TEA–HCl (pH 7.5) and 11 units of adenosine deaminase (calf intestine) were added, and the mixture was incubated at 30 °C for 7 h to quantitatively convert adenosine to inosine. Sodium arsenate (50 μL of 100 mM) and 0.38 unit of purine nucleoside phosphorylase (bovine spleen) were added, and the solution was incubated overnight at 30 °C. HPLC analysis indicated complete arsenolysis of inosine to hypoxanthine. The solution containing the labeled hypoxanthine was dried under vacuum, resuspended in 250 μL of 1.3 mM hypoxanthine (unlabeled), and purified by HPLC (4.6 × 100 mm Waters μBondapak C_{18} column; mobile phase, 25 mM ammonium phosphate (pH 5.0); flow rate, 1.0 mL/min). Purified, labeled hypoxanthine was dried under vacuum, resuspended in 300 μL of 50 mM triethanolamine-HCl pH 7.5, 1.2 units/mL xanthine oxidase (buttermilk), and incubated 24 h at 30 °C. The yield of urate from hypoxanthine was approximately 30% under these conditions. The labeled urate was purified by HPLC using the ammonium phosphate system described above. The purified, labeled urate was dried under vacuum and resuspended in 300 μL of H_2O, the pH was adjusted to 7.5 with NaOH, 0.04 unit of uricase (porcine liver) was added, and the solution was incubated 5 h at 30 °C. The reaction mixture was applied to a column of G-10 Sephadex (1.5 × 90 cm, equilibrated with 20 mM acetic acid), and the allantoin and unreacted urate were eluted with 20 mM acetic acid. Fractions (1.0 mL) were collected and assayed for radioactivity, 245-nm absorbance, and allantoin. To assay column fractions for allantoin, an aliquot (20 μL) was dried on Whatman 3-mm paper and sprayed with Ehrlich's reagent (Smith, 1969). Each step in the conversion of AMP to allantoin was monitored by reverse-phase HPLC using authentic unlabeled nucleotide, nucleosides, or nucleobases as coelution standards.

Primary $^{15}(V_{max}/K_m)$ Isotope Effects. The $^{15}(V_{max}/K_m)$ isotope effects were determined by isotope ratio mass spectrometric analysis of ammonia (as N_2) from complete or partial conversion of AMP to ammonia by the use of natural abundance ^{15}N in AMP as the label. The complete conversion of AMP to IMP and NH_3 provides the $^{15}N/^{14}N$ ratio of the substrate. Conversion of 10-30% of AMP to IMP provided ammonia for the isotopic discrimination of $^{15}N/^{14}N$.

In a typical experiment using AMP as a substrate, 1-4 L of 50 mM HEPES, 150 μM AMP, and the desired concentration of ATP was adjusted to pH 10-12 with KOH. Solid KCl was added to bring the total K^+ to 100 mM. In some experiments, the potassium ion concentration was increased to 150 or 250 mM. Solutions were degassed to remove NH_3, the pH was adjusted to 7.0 with H_2SO_4, and dithiothreitol was added to 100 μM. AMP deaminase (6-40 ng/mL) was added and the extent of the reaction monitored by HPLC (Merkler & Schramm, 1987). Following conversion of 10–30% AMP to IMP, the reaction was stopped by the addition of H_2SO_4 to pH 2.5–3.0. In the reference samples, the reaction was continued until conversion of AMP to IMP was complete, followed by the addition of H_2SO_4 as above. The volumes of the acidic solutions were reduced to approximately 20 mL by rotary evaporation. The pH was adjusted to 11–12 with 5 M KOH, and the NH_3 was collected by steam distillation using a Kjeldahl apparatus (Kontes). The distillate was collected in dilute H_2SO_4. The ammonia was oxidized to N_2 and analyzed by isotope ratio mass spectrometry as described by Hermes et al. (1985). In some experiments, the initial concentration of AMP was 6.0 mM, and the initial volume of the reaction mixture was 25 mL. All reactions were carried out at 30 °C.

To measure the $^{15}(V_{max}/K_m)$ using ATP as a substrate, 100 mL of 50 mM HEPES (pH 7.0), 150 mM KCl, 30 mM ATP, and 100 μM dithiothreitol was sterilized by passage through a 0.2-μm filter into a sterile flask. The reaction was initiated by the addition of 4.5 μg/mL sterile yeast AMP deaminase followed by incubation for 5 days at 30 °C. The conversion of ATP to ITP was monitored by HPLC, and the NH_3 produced from ATP deamination was collected using the procedures outlined above. Controls without enzyme showed no conversion of ATP to ITP after 5 days at 30 °C. A second control contained all of the components for the reaction in addition to coformycin, a tight-binding inhibitor of AMP deaminase (Merkler et al., 1990). No conversion of ATP to ITP was detected after 5 days at 30 °C. These experiments are only feasible in the absence of added divalent metals, which catalyze the conversion of ATP to ADP. Free divalent cations are not required for AMP deaminase activity (Merkler et al., 1989).

Primary $^{14}(V_{max}/K_m)$ Isotope Effects. Primary $^{14}(V_{max}/K_m)$ isotope effects were determined by the double-isotope method. Enzyme was added to reaction mixtures containing both [6-^{14}C]AMP and [1′-^{3}H]AMP. Reaction mixtures of 80–600 μL containing 50 mM TEA–HCl (pH 7.0), 100 mM KCl, 100 μM dithiothreitol, 150 μM AMP, 0.1–0.4 μCi of [6-^{14}C]AMP, [1′-^{3}H]AMP and enzyme were incubated at 30 °C. In some experiments with AMP as substrate, 100 μM ATP or 113 μM GTP was included. At 3–60% conversion of AMP to IMP, the reaction mix was resolved on a C_{18} μBondapak column [0.2 × 30 cm; flow rate, 1.0 mL/min; mobile phase, 25 mM ammonium phosphate (pH 5.0)], and 1.0-mL fractions were collected directly into scintillation vials. Liquiscint (9.0 mL) was added to each fraction, and the fractions were counted. Fractions containing ≥95% of the total radioactivity in the IMP peak were counted for 10 min each for 6–10 repetitive cycles. No systematic variation was observed in counting efficiency over counting cycles. Scintillation counting and data analysis have been described for these techniques (Parkin et al., 1984).

Control experiments demonstrated that complete conversion of [1′-^{3}H]AMP and [6-^{14}C]AMP mixtures to IMP provided an isotope ratio ($^{3}H/^{14}C$) in the product that was unchanged from that in the starting substrate, within the standard error of the measurements. Control experiments containing no enzyme demonstrated that <0.2% of the labeled [6-^{14}C]AMP and [1′-^{3}H]AMP coeluted with IMP. Injection of control unlabeled reaction mixtures between experimental samples indicated that no radioactivity was carried over between samples in the HPLC analysis.

Calculation of Transition-State Structures. Kinetic isotope effects corresponding to specific transition-state structures were calculated using the BEBOVIB-IV program (Sims et al., 1977; Sims & Lewis, 1984). Because of the limitation on the number of atoms allowed in the calculations, 9-methyladenine was used as the reactant structure. The starting structure for the adenine portion of the substrate was taken from the X-ray crystal structure (Lai & Marsh, 1972). Hydrogen atoms were placed at their energetic minima. Atomic energy minimizations were carried out using the PM3 semiempirical molecular orbital procedure (Stewart, 1989), as implemented in the MOPAC 6.0 program package (Merz

& Besler, 1990). Acceptable transition states were those chemically reasonable structures whose calculated isotope effects matched the experimentally determined kinetic isotope effects [e.g., Horenstein et al. (1991)]. Bond force constants were derived from reported values (Sims & Lewis, 1984; Sims & Fry, 1974; Wilson et al., 1955).

Three transition-state models for the reaction mechanisms in Figure 1 were considered. In the first ($\dagger_1$ of Figure 1), the incoming nucleophile was modeled as a hydroxide ion placed at various distances from C6, while a full bond was retained to NH_2. The hybridization of C6 was converted incrementally from sp^2 to sp^3 as the C6–hydroxide bond was formed. For each C–O bond distance, the remainder of the molecule was minimized using MOPAC 6.0. This energy-minimized model was then used to calculate the isotope effects using BEBOVIB-IV. This method removes operator-induced bias for the assignment of total bond order to specific atoms and the assignment of bond lengths in transition-state structures containing a mixture of double, single, and partial bonds.

Transition states for the second case ($\dagger_2$ of Figure 1) had a full bond to the attacking oxygen nucleophile with sp^3-hybridized C6. The reaction coordinate was explored with decreasing bond orders to NH_3, while maintaining a full bond to O–C6. In this reaction coordinate, C6 proceeds from the sp^3 tetrahedral intermediate in increments toward sp^2 at C6 hybridization as the C6–NH_3 bond order decreases. The transition states for the concerted mechanism ($\dagger_c$ of Figure 1) had decreased C6–NH_3 bond order as C6–O bond order increased, to maintain a constant C6–NH_3 + C6–O bond order. For each transition-state structure, the remaining atoms of the molecule were minimized using MOPAC 6.0 before being used as the transition-state structures in BEBOVIB-IV calculations, as described above.

RESULTS

Synthesis and Structure of [6-^{14}C]AMP. AMP labeled specifically in the 6-position is necessary to permit measurement of the primary 6-^{14}C kinetic isotope effect with AMP. The compound was synthesized from [6-^{14}C]adenine and 5-phosphoribose-1-pyrophosphate with adenine phosphoribosyl transferase. To test the isotopic integrity of the molecule, a portion of the same preparation of [6-^{14}C]AMP used for the kinetic isotope effects was degraded to allantoin. Stepwise enzymatic conversion of [6-^{14}C]AMP to allantoin released only C6 from the purine ring, thus providing convenient verification of the position of the radioactive label. In the final step in the analysis, allantoin was purified on G-10 Sephadex (Figure 3). There was no radioactivity above background associated with allantoin generated from the [6-^{14}C]AMP. Thus, only the carbon atom at C6 was radiolabeled in the [6-^{14}C]AMP.

^{15}N Primary Kinetic Isotope Effects. With AMP as substrate at a low concentration of 150 μM, the $^{15}(V_{max}/K_m)$ increased from 1.008 ± 0.003 to 1.016 ± 0.003 as ATP was increased from 0 to 100 μM. The difference between these mean values is highly significant at the <0.001 probability level using the student's *t*-test (Volk, 1969). Over the concentration range of 0 to 100 μM ATP, the $S_{0.5}$ for ATP decreased from 1.35 to 0.21 mM. ATP is known to allosterically affect the catalytic efficiency of subunits at low substrate levels (Merkler et al., 1989). Allosteric transitions have previously been reported to change transition-state structure and, thus, observed isotope effects (Mentch et al., 1987). At a high substrate concentration of 6 mM, the addition of 750 μM ATP had no significant effect on the reaction rate or on $^{15}(V_{max}/K_m)$. Under conditions of near-saturating substrate, ATP binding to the enzyme still occurs (Merkler & Schramm, 1990). The experimental values for $^{15}(V_{max}/K_m)$ at 6 mM AMP ± ATP were not significantly different from those obtained at 150 μM AMP with no ATP (Table I). The average $^{15}(V_{max}/K_m)$ for AMP deamination in the absence of ATP was 1.009 ± 0.002. Use of D_2O as solvent resulted in an average $^{15}(V_{max}/K_m)$ of 1.007 ± 0.002. Comparison of the $^{15}(V_{max}/K_m)$ values in H_2O and D_2O at 6 mM AMP without ATP gave values of 1.011 ± 0.001 and 1.007 ± 0.002, respectively (Table I). When the observed errors of 0.001 and 0.002 for these values are used, the probability of the values being the same is at the 0.001 level. However, these values differ only at the 0.2 confidence level using the student's *t*-test and the average error of 0.003 observed in Table I for this experimental method. When ATP was used as a poor substrate, the $^{15}(V_{max}/K_m)$ was 1.013 ± 0.001, which is similar to the values of 1.014 ± 0.005 and 1.016 ± 0.003 found with low AMP in the presence of ATP. The average of the

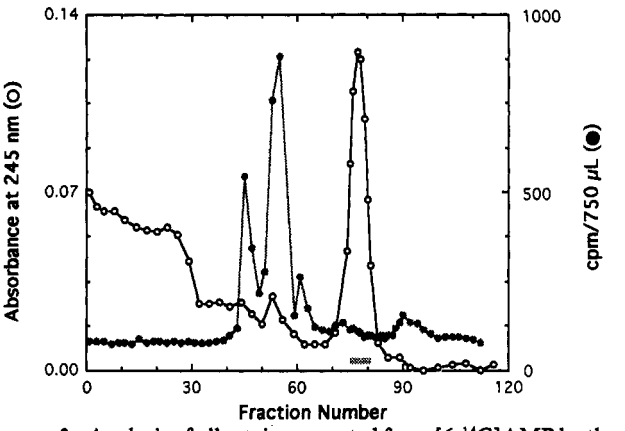

FIGURE 3: Analysis of allantoin generated from [6-^{14}C]AMP by the procedure in Figure 2. The reaction mixture for conversion of urate to allantoin was eluted from G-10 Sephadex. The allantoin was detected in fractions 75-81 using Ehrlich's reagent, as indicated by the stippled bar and the absorbance at 245 nm. No significant radioactivity was associated with the allantoin. The major radioactivity at tube 55 is associated with unreacted urate which retains ^{14}C (see Figure 2). The shoulder peaks likely represent labeled bicarbonate salts. Most of the ^{14}C is lost as $^{14}CO_2$ under the conditions of chromatography.

Table I: Primary $^{15}(V_{max}/K_m)$ Kinetic Isotope Effects

experiment	substrate	ATP[a] (μM)	solvent	$^{15}(V_{max}/K_m)$	n[b]
	Effect of Allosteric Activation				
1	150 μM AMP	0	H_2O	1.008 ± 0.003	8
2	150 μM AMP	1.5	H_2O	1.014 ± 0.005	5
3	150 μM AMP	100	H_2O	1.016 ± 0.003	5
	Effect of High Substrate Concentration				
4	6.0 mM AMP	0	H_2O	1.011 ± 0.001	5
5	6.0 mM AMP	750	H_2O	1.008 ± 0.002	3
	Effect of D_2O				
6	6.0 mM AMP	0	D_2O	1.007 ± 0.002	3
	Effect of Slow Substrate				
7	30 mM ATP		H_2O	1.013 ± 0.001	2
	average of 1 and 4			1.009 ± 0.002[c]	13
	average of 2, 3, and 7			1.014 ± 0.003[d]	12

[a] Concentration of ATP included in the assay when AMP is the substrate. [b] Number of determinations. [c] Average of the $^{15}(V_{max}/K_m)$ isotope effects for AMP in the absence of allosteric activation by ATP. [d] Average of the $^{15}(V_{max}/K_m)$ isotope effects for AMP in the presence of ATP activation (2 and 3) and for 30 mM ATP, where both the substrate and catalytic sites are saturated with ATP.

Table II: Primary $^{14}(V_{max}/K_m)$ Kinetic Isotope Effects[a]

experiment	addition	$^{14}(V_{max}/K_m)$	n^b
1	none	1.030 ± 0.003	17
2	100 μM ATP	1.038 ± 0.004	10
3	113 μM GTP	1.042 ± 0.003	9
4	control[c]	1.001 ± 0.003	13
average of 2 and 3		1.040 ± 0.003	19

[a] AMP concentrations were fixed at 150 μM plus labeled AMP to give final concentrations near 200 μM. [b] Number of determinations. [c] Ratio of $^3H/^{14}C$ of the substrate in the absence of AMP deaminase to the $^3H/^{14}C$ ratio of the product for 100% conversion of labeled AMP to IMP.

$^{15}(V_{max}/K_m)$ values for reactions in the presence of ATP was 1.014 ± 0.003 (Table I).

^{14}C Primary Kinetic Isotope Effects. In the absence of allosteric effectors, the hydrolysis of AMP gave a primary $^{14}(V_{max}/K_m)$ isotope effect of 1.030 ± 0.003. Similar to the pattern for the $^{15}(V_{max}/K_m)$ effects, the $^{14}(V_{max}/K_m)$ value obtained in the presence of allosteric activation by ATP was 1.038 ± 0.004. In the presence of the allosteric inhibitor, GTP, the value was 1.042 ± 0.003. The average of the ^{14}C kinetic isotope effects under the influence of allosteric modification was 1.040 ± 0.003 (Table II).

A control experiment for the double-labeled radioisotope method was conveniently obtained by comparing the observed ratio of $^3H/^{14}C$ in starting AMP to that in IMP following complete enzymatic conversion of AMP to IMP. This control corrects for impurities in substrates and for changes induced by chemical quenching of IMP relative to AMP in $^3H/^{14}C$ detection. Experiment 4 of Table II illustrates that both AMP and IMP gave equivalent values in counting $^3H/^{14}C$ ratios.

Transition-State Analysis. Transition-state analysis for yeast AMP deaminase was limited to the experimental conditions that gave the maximum kinetic isotope effects. These are conditions of AMP hydrolysis where the enzyme is under the influence of the allosteric effectors ATP or GTP or where ATP is used as a slow substrate. Isotope effects obtained under these conditions are not significantly different at a mean error of 0.003 and were averaged to give 1.014 ± 0.003 for $^{15}(V_{max}/K_m)$ in Table I and 1.040 ± 0.003 for $^{14}(V_{max}/K_m)$ in Table II. Three simplified reaction coordinate diagrams for the AMP deaminase reaction are shown in Figure 4. The figure to the left shows the energetically unfavorable step as attack of the zinc-activated water, leading to the formation of a covalent intermediate with fully bonded hydroxyl and amino groups at C6 which is rehybridized to sp^3. In this mechanism, the kinetic isotope effects report on the transition state formed by hydroxyl attack on the path to formation of the intermediate, while the exocyclic ammonium

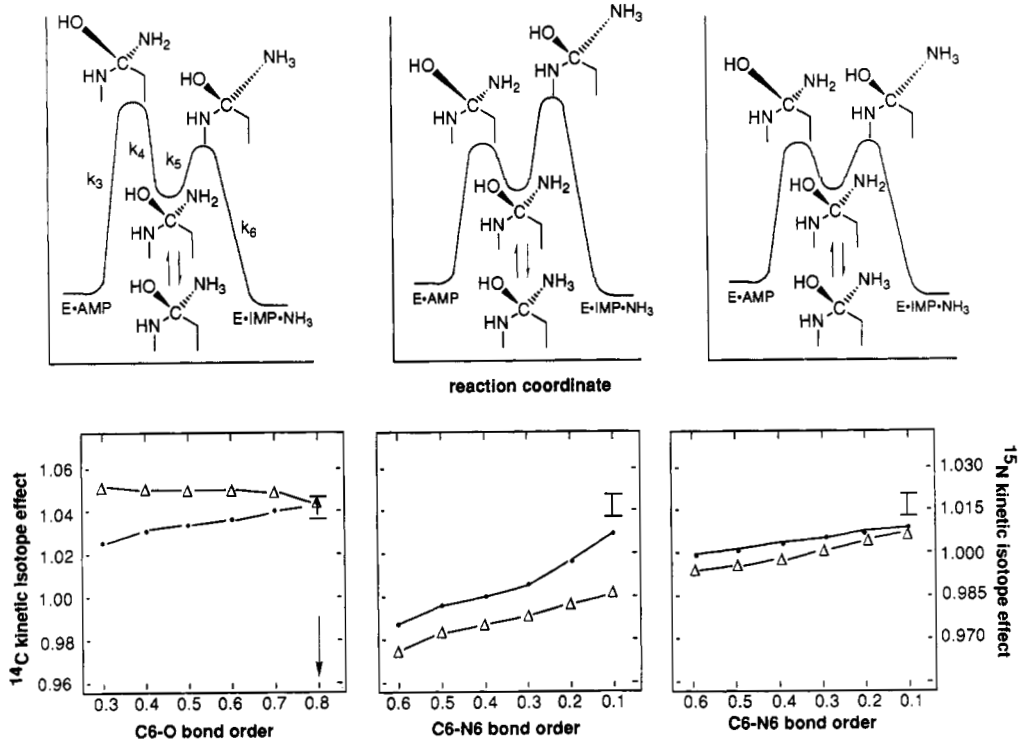

FIGURE 4: Calculated isotope effects as a function of transition-state structure. The upper panels illustrate hypothetical reaction coordinates with energetically unfavorable attacks of the $ZnOH^-$ before formation of an sp^3 intermediate (upper left), rate-limiting departure of NH_3 from the sp^3 intermediate (upper center), and a mechanism with equal energetic barriers for OH attack and NH_3 departure (upper right). Although protonation is shown as a reversible step perpendicular to the intermediate, protonation occurs sequentially as a prior equilibrium before the molecule progresses through step k_5 of the reaction. The lower panels illustrate the ^{14}C and ^{15}N kinetic isotope effects expected for the reaction mechanisms with the energetic barriers shown above. The kinetic isotope effects were determined by a combination of MOPAC-6 and BEBOVIB-IV calculations as a variation of C6–O and C6–N bond orders at the indicated transition states. The solid lines indicate the calculated kinetic isotope effects for the bond orders indicated on the abscissae. The ordinate scales have been adjusted so that the experimental values for $^{14}(V_{max}/K_m)$ of 1.040 ± 0.003 (Table II) and $^{15}(V_{max}/K_m)$ of 1.014 ± 0.003 (Table I) are coincident in the indicated bar. The limits of the bar indicate the standard error associated with the isotope effect measurements. The experimental isotope effect value was placed where it corresponds most closely to the calculated isotope effects for proposed transition states. The C6–O bond orders were fixed as shown (lower left), and the C6–N6 and other bond orders were calculated by MOPAC-6 prior to calculation of the isotope effects. The C6–N6 bond order varied from 1.32 to 1.05 as the C6–O bond order varied from 0.1 to 0.8. For the calculations in the middle panel (lower), the C6–N6 bond order was fixed at the values indicated, the C6–O and other bonds were determined by MOPAC-6 calculations, and the resulting structures were used to calculate the kinetic isotope effects. Kinetic isotope effect calculations for the mechanism on the upper right fixed the C6–O bond order at 0.8 and the C6–N bond orders as indicated on the abscissa and calculated the bond lengths for the minimum-energy structure of the remainder of the molecule using MOPAC-6. The resultant structure was used for BEBOVIB-IV calculations. For all MOPAC-6 and BEBOVIB-IV calculations, the molecule contained all atoms of 9-methyladenine in addition to the changes indicated above.

remains fully bonded as NH_2. Using the molecular vibrational modeling methods described in the Materials and Methods section, a transition-state structure consistent with the isotope effects was found with a bond order to the attacking water oxygen of between 0.7 and 0.9. The NH_2 experiences bonding changes at the transition state of this mechanism due to the rehybridization of C6 to near-sp^3 geometry. Protonation of NH_2 to NH_3 does not occur until after formation of the unstable tetrahedral intermediate.

Formation of bonded NH_3 at the transition state is inconsistent with this mechanism since the increased bond order to the exocyclic nitrogen would decrease the size of the ^{15}N isotope effect to a value well below the experimental value. The mechanism requires two additional rapid steps for decomposition of the intermediate: protonation of NH_2 to form NH_3 and NH_3 departure. Reaction coordinate motion for this transition state involves O→C bond approach with coupled conversion of sp^2 geometry at C6 to sp^3 as the O–C bond forms.

The center panel in Figure 4 illustrates a reaction coordinate with facile addition of the zinc-activated hydroxyl to form a quasi-stable intermediate. In order for NH_2 to leave, it must be protonated to NH_3 in an equilibrium step before C–N bond loss begins. In this case, the equilibrium isotope effects for NH_2 to NH_3 and C6-sp^2 to C6-sp^3 conversions must be included in the formation of the intermediate, since ^{15}N and ^{14}C isotopic fractionations will have already occurred for the species prior to crossing the highest energy barrier of the reaction coordinate (Weiss et al., 1987). The kinetic isotope effects in this mechanism arise from rehybridization of C6 and C6–N bond loss.

The reaction coordinate illustrated in the upper right panel of Figure 4 is characterized by approximately equal energy barriers for hydroxyl addition and NH_3 departure, with the tetrahedral intermediate poised in between. Formation of the tetrahedral intermediate and its breakdown occur at approximately equal rates; thus, neither formation nor breakdown of the intermediate is rate-limiting. The protonation of NH_2 occurs in an equilibrium step prior to NH_3 departure. This reaction mechanism is similar to that proposed by Weiss et al. (1987) for the reaction of adenosine with adenosine deaminase.

Not shown in the reaction coordinates of Figure 4 are the substrate-binding step and the proton transfers from zinc-activated water and from Glu633 to N1 of AMP, which are required prior to attack of the hydroxide. These have no influence on $^{14}(V_{max}/K_m)$ and $^{15}(V_{max}/K_m)$; since their transfer is remote from the 6-amino group, they occur as equilibrium steps and, for the slow substrate deoxyadenosine monophosphate, are complete before hydroxyl addition (Merkler & Schramm, 1993). The panels below the reaction coordinate diagrams indicate the calculated and observed kinetic isotope effects for [6-^{14}C]AMP and [6-^{15}N]AMP for each of the reaction coordinates shown above. Agreement between the observed and calculated kinetic isotope effects occurs only for the case where the largest energy barrier in the reaction is the attack of the hydroxyl on C6.

DISCUSSION

Analysis of ^{15}N and ^{14}C Kinetic Isotope Effects for Yeast AMP Deaminase. The equations for deamination of adenosine by adenosine deaminase have been presented for ^{15}N kinetic isotope effects (Weiss et al., 1987) and can also be applied to the ^{15}N and ^{14}C kinetic isotope effects reported here. For AMP deamination with an intermediate, the steps are as follows:

$$E + AMP \underset{k_2}{\overset{k_1}{\rightleftharpoons}} E{\cdot}H_2AMP \underset{k_4}{\overset{k_3}{\rightleftharpoons}} E{\cdot}HO{\cdot}AMP_{sp^3} \underset{k_6}{\overset{k_5}{\rightleftharpoons}} E{\cdot}IMP{\cdot}NH_3 \quad (1)$$

Analysis of this mechanism using the slow substrate, deoxyadenosine monophosphate, indicated that two or more proton transfers occur prior to formation of the tetrahedral intermediate, on the basis of a D_2O proton inventory (Merkler & Schramm, 1993). These transfers result in an inverse solvent isotope effect that is largest with slow substrates, but is also inverse with AMP. These results indicate that proton transfers do not dominate the prominent energetic barriers in the reaction coordinate, since transfers at energetic barriers result in normal solvent deuterium isotope effects. The more modest inverse solvent D_2O isotope effects observed with AMP as substrate permit a mixture of proton transfer *and* inverse equilibrium isotope effects to contribute to the observed isotope effects, provided that the inverse, equilibrium effects dominate. Similar mechanisms have been considered by Kiick (1991).

A tetrahedral intermediate with fully bonded hydroxyl and amino groups is postulated ($E{\cdot}HO{\cdot}AMP_{sp^3}$) because of the arguments that can be raised against a classical concerted mechanism (see below). This intermediate is formed at the rate k_3 and decomposes either to substrate (k_4) or to enzyme-bound products (k_5). The reverse reaction for AMP deaminase has not been demonstrated, despite efforts to measure it (Merkler et al., 1989); thus, the return reaction, k_6, can be eliminated from consideration. It is also assumed that binding of substrate does not significantly alter the bond vibrational modes of AMP and is thus isotopically silent [but see LaReau et al. (1989)]. Lack of isotopic effects on binding permits the elimination of k_1 and k_2 from the analysis.

The equation for the $^{15}(V_{max}/K_m)$ isotope effects under these conditions has been described (Weiss et al., 1987) as

$$^{15}(V/K) = \frac{(^{15}K_{eq})(^{15}k_5) + {}^{15}k_3(k_5/k_4)}{1 + k_5/k_4} \quad (2)$$

where $^{15}(V/K)$ is the observed ^{15}N kinetic isotope effect on V_{max}/K_m, $^{15}K_{eq}$ is the product of the ^{15}N equilibrium isotope effect of 0.9836 for converting NH_2 to NH_3 (Hermes et al., 1985) and the ^{15}N equilibrium constant between AMP and the tetrahedral intermediate, $^{15}k_5$ is the intrinsic ^{15}N kinetic isotope effect on the step that involves NH_3 loss, $^{15}k_3$ is the intrinsic ^{15}N kinetic isotope effect on the step leading to the formation of the tetrahedral intermediate, and k_5/k_4 is the probability that the tetrahedral intermediate will decompose to IMP and NH_3, relative to its return to AMP. Missing from eq 2 are rate terms for early protonations, since for the poor substrate, deoxyadenosine monophosphate, these are known to occur in equilibrium steps. The protonation which influences the $^{15}(V_{max}/K_m)$ is that for the conversion of NH_2 to NH_3 prior to NH_3 departure. The $^{15}K_{eq}$ term includes this transfer. Rates for other proton transfers can be eliminated since the solvent D_2O isotope effects for AMP deaminase are large and inverse for poor substrates and remain inverse, although less so for AMP, indicating that other proton transfers occur rapidly and are at or near equilibrium relative to the bond making and bond breaking steps. The relationship between the rate constants of eq 1 and the energetic barriers of the reaction mechanism for AMP deaminase are shown in the upper left panel of Figure 4.

Kinetic isotope effects report on the chemical bonding changes which occur at the highest energetic barriers on the

reaction coordinate and, in some cases, the reaction intermediates (Northrop, 1981). This relationship can be demonstrated for the AMP deaminase reaction by numerical analysis of eq 2. When k_5/k_4 is small, the $(^{15}K_{eq})(^{15}k_5)$ term dominates, while large values for k_5/k_4 cause $^{15}k_3$ to dominate. When $k_5 = k_4$, the $(^{15}K_{eq})(^{15}k_5)$ and $^{15}k_3$ terms contribute equally to the observed kinetic isotope effect. The $^{15}(V_{max}/K_m)$ value is influenced by $^{15}K_{eq}$ when protonation of NH_2 occurs before the rate-limiting step (center panel, top, Figure 4). When k_5/k_4 is large (upper left panel of Figure 4), proton transfer does not occur at the transition state and the observed isotope effects result from step k_3, hydroxyl attack leading to the tetrahedral intermediate.

The results in Figure 4 demonstrate that $^{15}(V_{max}/K_m)$ alone cannot resolve the relative heights of the reaction barriers. The D_2O solvent effects on $^{15}(V_{max}/K_m)$ for AMP deaminase are also too small to permit confident resolution of the relative reaction barriers. $^{14}(V_{max}/K_m)$ obtained with [6-^{14}C]AMP can be expressed in the same way as $^{15}(V_{max}/K_m)$, except that the term for NH_2 protonation no longer contributes and is replaced by a term for the equilibrium formation of the tetrahedral intermediate, $^{14}K_{eq}$:

$$^{14}(V/K) = \frac{(^{14}K_{eq})(^{14}k_5) + {}^{14}k_3(k_5/k_4)}{1 + k_5/k_4} \qquad (3)$$

Intrinsic ^{14}C kinetic isotope effects are expressed at large k_5/k_4 values, since an equilibrium is not established with the tetrahedral intermediates (upper left, Figure 4).

Elimination of a Concerted Reaction Mechanism. A concerted mechanism for yeast AMP deaminase can be eliminated from the combined results of the solvent D_2O and [6-^{15}N]- and [6-^{14}C]AMP isotope effects. Fully concerted mechanisms imply that all atomic motions that occur during catalysis are participating at the transition state. During deamination of AMP, a minimum of three proton transfers is required. Proton motion at a single, rate-limiting transition state would result in normal solvent D_2O isotope effects, unless all of the isotope effects were suppressed by a step which is isotopically silent. The observation of significant ^{15}N and ^{14}C V_{max}/K_m effects with inverse solvent D_2O effects (0.79 ± 0.11 for AMP; Merkler & Schramm, 1993) establishes that changes in bond order/hybridization at C6 do occur at the highest barrier(s) in the reaction coordinate. The essential proton transfers for this mechanism are not a major contribution to reaction coordinate motion at that step. Thus, a fully concerted mechanism is unlikely. A mechanism concerted only with respect to C–O bond making and C–N bond breaking would require protonation of NH_2 to initiate NH_3 loss. The magnitude of the ^{15}N isotope effect makes this possibility unlikely.

Evidence for Hydroxylation As the Highest Energetic Barrier. Comparison of the amino acid sequences for yeast AMP deaminase and mouse adenosine deaminase reveals strong conservation of the amino acid residues known to form the contacts in the crystal structure of the mouse enzyme with the 6-hydrate of purine riboside (Wilson et al., 1991; Merkler & Schramm, 1993). On the basis of this homology, the catalytic mechanisms are likely to be related for mammalian adenosine deaminases and yeast AMP deaminase. Earlier studies have established that the V_{max} rates for hydrolysis of adenosine and 6-chloropurine riboside are within an order of magnitude for fungal and calf intestinal adenosine deaminases (Chassey & Suhadolnik, 1967; Baer et al., 1968). This finding is remarkable, considering the estimated difference of 16 kcal/mol in the free energy of hydrolysis for adenosine and 6-chloropurine riboside (Wolfenden, 1969), and has been interpreted as the rate-limiting formation of a tetrahedral intermediate, with rapid departure of the leaving group. This result is also consistent with crystallography studies, which show a remarkably open space near the expected position for the NH_3 leaving group (Wilson et al., 1991). Even the proton donor proposed to form the departing NH_3, the His238 of adenosine deaminase, is "less than ideal for proton transfer" at 4.5 Å (Wilson & Quiocho, 1993). Thus, the catalytic machinery is designed to form a reactive hydroxyl and to position it close to the reaction center.

Rate-limiting formation of a tetrahedral intermediate is shown in the upper left panel of Figure 4. Since the attack of hydroxyl forms a transition state prior to NH_2 protonation, the kinetic isotope effects arise from the quasi-equilibrium between AMP and the attack of the zinc-activated water. In this case, the $^{15}k_3$ and $^{14}k_3$ terms dominate in eqs 2 and 3. In X-ray crystal studies of adenosine deaminase with 1-deazaadenosine, the Zn–O bond distance is 1.91 Å, consistent with the formation of a zinc hydroxide prior to attack at C6 (Wilson & Quiocho, 1993). Both the ^{14}C and ^{15}N kinetic isotope effects agree with a late transition state, with a C6–O bond order near 0.8 ± 0.1, on the path to formation of the tetrahedral intermediate. Subsequent protonation and departure of the exocyclic amine must be rapid. For the observed kinetic isotope effects to result only from the hydroxyl attack, subsequent steps must be greater than 10-fold faster than hydroxyl attack.

The change in the inverse solvent isotope effect, from 0.34 ± 0.02 for the poor substrate dAMP to 0.79 ± 0.11 for AMP, indicates that a 2-fold normal solvent deuterium isotope effect could be expressed as part of the reaction coordinate motion. A 2-fold effect would be observed by an asymmetric transfer of a proton from Glu633 to N1 which is nearly, but not quite, complete at the highest barrier shown in the upper left panel of Figure 4. Since the attack of OH is approximately 80% complete, protonation at N1 might also be expected to be approximately 80% complete at the highest energetic barrier.

A mechanism that leads to the formation of a tetrahedral intermediate followed by a slow departure of NH_3 is illustrated in the upper middle panel of Figure 4. The observed isotope effects for this mechanism involve the equilibrium isotope effects between substrate and tetrahedral intermediate, as well as the kinetic isotope effects of k_5. When the isotope effects are calculated for this mechanism (see legend to Figure 4) as a function of C6–N bond breaking, the results are in poor agreement with the experimentally determined isotope effects (lower middle panel, Figure 4). This result was obtained with the assumption that $k_5/k_4 < 0.1$. Alteration of this ratio from 0.01 to 1.0 does not provide agreement between the calculated and observed isotope effects. Thus, rapid formation of a tetrahedral intermediate followed by the slow departure of NH_3 is an unlikely mechanism.

When the ratio of $k_5/k_4 = 1$, the tetrahedral intermediate partitions equally to substrate and product (upper right panel, Figure 4). Under these conditions, isotope effects from k_3, k_5, and the equilibrium isotope effects of proton transfer to NH_2 all contribute to the observed values. With a fixed C6–O bond order of 0.8 for the first transition state and varied C6–N6 bond orders for the second transition state, the family of isotope effects in the lower right panel of Figure 4 can be calculated. The experimentally determined isotope effects are in poor agreement with these values, indicating that this reaction coordinate is unlikely for yeast AMP deaminase.

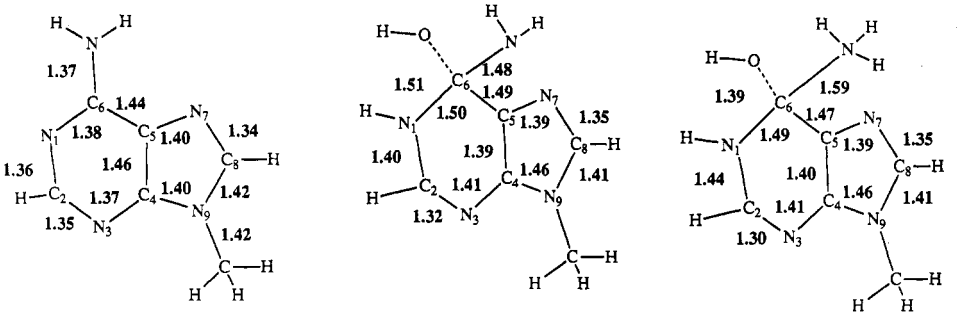

FIGURE 5: Bond lengths for ground-state (reactant) 9-methyladenine and the proposed transition states. The starting values for the structure of 9-methyladenine (left) were taken from the X-ray crystal structure (Lai & March, 1972). The structure was analyzed by MOPAC-6 to provide the positions and bonding to hydrogen atoms and the bond lengths shown above. The transition state labeled "OH attack transition state" and the "Energy-minimized intermediate" used the C6–OH and C6–NH_2 bond lengths from the BEBOVIB and/or MOPAC-6 calculations.

Bond Structure of the Transition State for AMP Deaminase. Bond vibrational structures for the AMP deaminase reaction used 9-methyladenine to simplify calculations. Isotope effects calculated from bond vibrational considerations are independent of substitutions more than two bonds away from the site of isotopic substitution (Sims & Lewis, 1984). The bond lengths for the ground-state molecule were estimated by MOPAC calculations using the X-ray crystal structure as the starting point (Lai & Marsh, 1972). This approach provides the bond lengths shown in Figure 5 (left) for the adenine ring prior to interaction with the enzyme. The transition state consistent with both ^{14}C and ^{15}N kinetic isotope effects has a well-developed bond of 1.51 Å with the attacking hydroxyl. Although the C6–N6 retains much of its bond character, the bond is considerably destabilized by the hydroxyl attack, increasing from 1.37 to 1.48 Å (middle structure, Figure 5). Departure of the amino group requires protonation to NH_3, which further destabilizes the C6–N6 bond to 1.59 Å, corresponding to a bond order of 0.7 (right structure, Figure 5). This intermediate is sufficiently destabilized to cause the rapid loss of NH_3, with a low probability of return to the Michaelis complex. Formation of an sp^3 center at C6 causes loss of the aromatic character of the pyrimidine ring, leading to significant ring expansion. The N1–C6 bond length increases from 1.38 to 1.50 Å at the transition state. These features explain the tight binding of the (*R*)-coformycin analogues, since the 7-membered ring places the hydroxyl in a position similar to that of the attacking hydroxyl in the transition state without positive charge in the location of the departing NH_3 (Merkler et al., 1990; Frieden et al., 1980). If the NH_3^+ were a dominant feature of the transition state, inhibitors (like coformycin) which are missing this charge would be unlikely to act as transition-state inhibitors [e.g., Horenstein and Schramm (1993)].

Conclusions. Comparison of experimental and calculated ^{14}C and ^{15}N kinetic isotope effects for yeast AMP deaminase indicates that the largest energetic barrier is hydroxyl attack at C6. This transition state is achieved prior to NH_2 protonation. This mechanism is consistent with the interaction of coformycin transition-state inhibitors and with the crystal structure of the related enzyme, adenosine deaminase.

ACKNOWLEDGMENT

The authors thank Dr. W. W. Cleland for a critical reading of the manuscript and Dr. R. Wolfenden for helpful discussions. We thank Dr. Flo Quiocho for providing the coordinates for adenosine deaminase with the bound hydrate of purine riboside and Dr. James Sacchettini for his help in computer modeling of the transition-state structure into the crystal structure of adenosine deaminase.

REFERENCES

Baer, H. P., Drummond, G. I., & Gillis, J. (1968) *Arch. Biochem. Biophys. 123*, 172–178.
Chaney, A. L., & Marback, E. P. (1962) *Clin. Chem. 8*, 130–132.
Chassy, B. M., & Suhadolnik, R. J. (1967) *J. Biol. Chem. 242*, 3655–3658.
Frieden, C., Kurz, L. C., & Gilbert, H. R. (1980) *Biochemistry 19*, 5303–5309.
Hermes, J. D., Weiss, P. M., & Cleland, W. W. (1985) *Biochemistry 24*, 2959–2967.
Horenstein, B. A., & Schramm, V. L. (1993) *Biochemistry 32*, 7089–7097.
Horenstein, B. A., Parkin, D. W., Estupinan, B., & Schramm, V. L. (1991) *Biochemistry 30*, 10788–10795.
Kiick, D. M. (1991) *J. Am. Chem. Soc. 113*, 8499–8504.
Kurz, L. C., Moix, L., Riley, M. C., & Frieden, C. (1992) *Biochemistry 31*, 39–48.
Lai, T. F., & Marsh, R. E. (1972) *Acta Crystallogr. B28*, 1982–1989.
LaReau, R., Wah, W., & Anderson, V. (1989) *Biochemistry 28*, 3619–3624.
March, J. (1984) *Advanced Organic Chemistry*, 3rd ed., pp 576–607, John Wiley & Sons, New York.
Mentch, F., Parkin, D. W., & Schramm, V. L. (1987) *Biochemistry 26*, 921–930.
Merkler, D. J., & Schramm, V. L. (1987) *Anal. Biochem. 167*, 148–153.
Merkler, D. J., & Schramm, V. L. (1990) *J. Biol. Chem. 265*, 4420–4426.
Merkler, D. J., & Schramm, V. L. (1993) *Biochemistry 32*, 5792–5799.
Merkler, D. J., Wali, A. S., Taylor, J., & Schramm, V. L. (1989) *J. Biol. Chem. 264*, 21422–21430.
Merkler, D. J., Brenowitz, M., & Schramm, V. L. (1990) *Biochemistry 29*, 8358–8364.
Merz, K. M., Jr., & Besler, B. H. (1990) *Quantum Chemistry Program Exchange*, No. 589, Indiana University, Bloomington, IN.
Meyer, S. L., Kvalnes-Krick, K. L., & Schramm, V. L. (1989) *Biochemistry 28*, 8734–8743.
Murakami, K. (1979) *J. Biochem. (Tokyo) 86*, 1331–1336.
Northrop, D. B. (1981) *Annu. Rev. Biochem. 50*, 103–131.
Parkin, D. W., Leung, H. B., & Schramm, V. L. (1984) *J. Biol. Chem. 259*, 9411–9417.

Scharff, A. J., Wilson, D. K., Chang, Z., & Quiocho, F. A. (1992) *J. Mol. Biol. 226*, 917–921.
Sims, L. B., & Fry, A. (1974) *Special Publication No. 1.*, University of Arkansas, Fayetteville, AR.
Sims, L. B., & Lewis, D. E. (1984) *Isot. Org. Chem. 6*, 161–259.
Sims, L. B., Burton, G. W., & Lewis, D. E. (1977) *BEBOVIB-IV, Quantum Chemistry Program Exchange*, No. 337, Indiana University, Bloomington, IN.
Smith, I. (1969) in *Chromatographic and Electrophoretic Techniques*, 3rd ed., (Smith, I., Ed.) Vol. 1, pp 118–121, Pitman Press, Bath, UK.
Stewart, J. J. P. (1989) *Comput. Chem. 10*, 209–220.
Volk, W. (1969) in *Applied Statistics for Engineers*, 2nd ed. pp 127–133, McGraw-Hill, New York.
Weiss, P. M., Cook, P. F., Hermes, J. D., & Cleland, W. W. (1987) *Biochemistry 26*, 7378–7384.
Wilson, D. K., & Quiocho, F. A. (1993) *Biochemistry 32*, 1689–1694.
Wilson, E. B., Decius, J. C., & Cross, P. C. (1955) *Molecular Vibrations*, McGraw-Hill Book Co., Inc., New York.
Wilson, D. K., Rudolph, F. B., & Quiocho, F. A. (1991) *Science 252*, 1278–1284.
Wolfenden, R. (1969) *Biochemistry 8*, 2409–2412.
Yeung, C. Y., Ingolia, D. E., Roth, D. B., Shoemaker, C., Al-Ubaidi, M. R., Yen, J. Y., Ching, C., Bobonis, C., Kaufman, R. J., & Kellams, R. E. (1985) *J. Biol. Chem. 260*, 10299–10307.
Yoshino, M., & Murakami, K. (1980) *Biochim. Biophys. Acta 616*, 82–88.
Yoshino, M., & Murakami, K. (1986) *Int. J. Biochem. 18*, 235–239.
Yoshino, M., & Murakami, K. (1988) *Biochim. Biophys. Acta 954*, 271–276.
Yoshino, M., Murakamai, K., & Tsushima, K. (1979) *Biochim. Biophys. Acta 570*, 157–166.